PAPER

Check for updates

Ultrafast ambipolar switching in electrochromic copolymer thin films of zinc(II) tetrakis(4-aminophenyl)porphyrin – 3,4-ethylenedioxythiophene

Sachin Kochrekar, [ID] *[ab] Subrahmanyam Sappati, [ID] [cd] Plawan Kumar Jha, [ID] [b] Ermei Mäkilä, [ID] [e] Ashwini Jadhav, [ID] [ab] Pia Damlin, [ID] [b] Mikko Salomäki [ID] [b] and Carita Kvarnström [ID] *[b]

Electrocopolymerization of different monomers is a useful approach for developing materials with tailored electrochromic properties and expanded color palettes. We report electrocopolymerization of two distinct monomers – zinc(II) tetrakis(4-aminophenyl)porphyrin (ZnTAPP) and 3,4-ethylenedioxythiophene (EDOT) on an FTO-coated glass substrate. Our copolymer, poly(ZnTAPP–EDOT), exhibits a reversible color change from orange-brown to olive-green, with optical contrasts of 25% and 31% in the visible and beginning of the near-IR (bNIR) regions, respectively. It also demonstrates high coloration efficiencies of 434 cm^2 C^{-1} (visible region) and 181 cm^2 C^{-1} (bNIR region). Furthermore, poly(ZnTAPP–EDOT) retains 88% of its electrochromic performance in the visible and 82% in the bNIR regions after 200 redox cycles, along with a fast switching response and strong optical memory under open-circuit conditions. Our time-dependent density functional theory (TDDFT) calculations reveal that the increasing EDOT units between ZnTAPP moieties promote a systematic redshift in absorption peaks and enhance oscillator strengths, attributed to extended π-delocalization facilitated by the added EDOT linkages, corroborating experimental UV-vis data. Our results suggest that the electrocopolymerization of suitable porphyrins with selective monomers can produce electrochromic materials with tunable optical properties, high efficiency, and stability, making them well-suited for use in electrochromic devices.

1. Introduction

Color is a prominent visual feature in nature, and the ability to induce or undergo color change is both biologically significant and scientifically intriguing.[1] This dynamic interplay of colors can also be triggered in chromic materials by external stimuli such as light, temperature, pressure, chemical environment, or electric field. Among these, the electric field offers distinct advantages, including precise control, rapid response, environmental adaptability, and low energy consumption. The phenomenon induced by the electric field is called electrochromism.[2] Electrochromic (EC) materials are at the forefront of research and development due to their ability to reversibly modulate optical properties through redox-driven electronic changes.[3–5] These materials have progressed significantly, demonstrating promising commercial potential in applications such as low-energy and color-tunable displays, smart windows, electronic papers, military camouflage devices, and energy-efficient glasses.[6–9] EC materials are broadly classified as organic and inorganic materials.[3] Inorganic EC materials include transition metal oxides and hexacyanometallates, whereas organic EC materials consist of small organic molecules, conjugated polymers, and covalent organic frameworks.[3,7,10] Organic EC materials offer significant advantages, including ease of fabrication, fast response times, and rich color palettes. However, they suffer from inferior durability and chemical stability.[4,7,11] Recent research aimed at overcoming these limitations and realizing their full commercial potential is noteworthy. Among organic materials, conjugated polymers have attracted particular interest due to their reversible optical behavior under applied electric fields. These polymers possess flexibility, well-defined redox states, excellent processability, and the ability to exhibit multiple

[a] *Turku University Graduate School (UTUGS) Doctoral Programme in EXACTUS, FI-20014 Turku, Finland. E-mail: spkoch@utu.fi*

[b] *Department of Chemistry, University of Turku, Henrikinkatu 2, FI-20500 Turku, Finland. E-mail: carkva@utu.fi*

[c] *Department of Pharmaceutical Technology and Biochemistry, Gdańsk University of Technology, Gabriela Narutowicza 11/12, Gdańsk, 80-233, Poland*

[d] *BioTechMed Center, Gdańsk University of Technology, Gabriela Narutowicza 11/12, Gdańsk, 80-233, Poland*

[e] *Laboratory of Industrial Physics, Department of Physics, University of Turku, Turku FI-20014, Finland*

This journal is © The Royal Society of Chemistry 2025

J. Mater. Chem. C, 2025, **13**, 23577–23588 | **23577**

distinct colors. They also offer high optical contrast, improved switching reproducibility, and long lifetimes.[10–13] A significant number of research studies have focused on designing and improving EC polymers with specific structural and optical characteristics.[14,15] To achieve multichromatic behavior, a range of synthetic strategies has been developed. The most common approaches involve modifying the monomer units, followed by either homopolymerization or copolymerization of different monomers.[13] Copolymerization can be a practical and straightforward method for producing random, alternating, or periodic copolymers with intriguing multi-EC properties.[13,15] EC copolymers can be synthesized by both chemical and electrochemical methods.[16] The chemical route is advantageous for large-scale production; however, it sometimes requires corrosive transition metal salts, toxic solvents, and time-consuming procedures. In contrast, electrochemical methods generally avoid the use of such salts and solvents, and offer better control, easier synthesis, and structurally diverse EC polymers.[17]

Poly(3,4-ethylenedioxythiophene) (PEDOT) and its derivatives are among the most extensively studied conducting polymers, owing to their low oxidation potentials, fast switching kinetics, environmental stability, high energy HOMO levels, and remarkable optical and electronic properties.[15,18] The electrocopolymerization of EDOT with thiophene, carbazole, pyrrole, indole, and aniline was widely explored for EC applications.[4,18–21] Beyond these conventional monomers, porphyrins, which are an 18π delocalized electron system, could be a classic choice due to their significant emission and absorption characteristics.[22,23] Porphyrins also represent a promising class of electroactive building blocks.[15] In addition, porphyrins are amenable to functionalization, enabling synergistic interactions through coordinating with different metal centers, expanding colour tunability.[24,25] Several studies have reported porphyrin-based electroactive polymers with optimized multifunctional performance, particularly those synthesized electrochemically.[26–29] For instance, Cogal *et al.* electrocopolymerized 2-thienyl-substituted porphyrins with 3-alkylthiophene to investigate their EC behavior.[27] Likewise, multi-step chemical synthesis followed by electropolymerization has been used to construct porphyrin-based copolymers for EC applications.[22,24,30,31] More recently, Guo *et al.* reported a series of electrocopolymers based on four *meso*-tetrakis(thienyl) porphyrins copolymerized with EDOT and thiophenes, demonstrating multi-EC behavior.[15] Despite progress in porphyrin-based electroactive polymers, many *meso*-substituted metalloporphyrins copolymerized with EDOT remain underexplored as EC materials, leaving substantial scope to improve switching speed, chromic memory, broaden the color palette, and extend absorption into the beginning of the near-IR (bNIR) region. 5,10,15,20-Tetrakis(2-aminophenyl)porphyrin (TAPP) represents an interesting class of *meso*-substituted porphyrins, in which electropolymerization proceeds *via* the nitrogen atom of the aminophenyl substituent at the *meso* position, while largely preserving the porphyrin π-system.[25,32,33] Although the electropolymerization of TAPP has been extensively studied, its copolymerization with EDOT and the consequent impact on its EC properties remain unexplored. In addition, their optical properties can be readily tuned through

metal coordination.[15,34] This approach, which combines the excellent conductivity and stability of PEDOT with the rich redox and optical properties of ZnTAPP, generates copolymer films with new hues and enhanced EC performance.

In this work, we report the electrocopolymerization of ZnTAPP and EDOT on FTO substrate. The similar onset potentials of EDOT and ZnTAPP enable efficient copolymerization through simultaneous radical formation. The resulting copolymer films (poly(ZnTAPP–EDOT)) were systematically characterized using microscopy, spectroscopy, and electrochemical techniques. The copolymer film showed rapid switching, high coloration efficiency (CE), and significant optical contrast in the Vis-bNIR regions. Furthermore, the material demonstrated excellent chromic memory under open-circuit conditions. Operando UV-Vis spectroscopy was employed to monitor the redox-dependent optical behavior. Density functional theory (DFT) and time-dependent DFT (TDDFT) calculations were performed to model propagation pathways and evaluate optical transitions. Overall, this study demonstrates the utility of electrocopolymerization as a robust platform for tailoring the EC and optoelectronic properties of porphyrin–EDOT systems, with clear potential for integration into next-generation EC devices.

2. Experimental section

2.1 Materials

All chemical reagents and solvents used were of analytical grade or higher. 5,10,15,20-Tetrakis(4-aminophenyl) porphyrin-Zn(II) (ZnTAPP) [Por-lab], 3,4-ethylenedioxythiophene (EDOT) [TCI, 98%], ferrocene [Aldrich, 99%], tetrabutylammonium hexafluorophosphate (TBAPF$_6$) [TCI, 98%] were used without further purification unless otherwise stated. TBAPF$_6$ was dried in a vacuum oven at 70 °C for 2 hours before use. Anhydrous acetonitrile (ACN) [Sigma-Aldrich, 99.9%] and dichloroethane (DCE) [Alfa Aesar, 99%] were distilled and stored in flasks containing 4 Å molecular sieves in a nitrogen-filled glove box.

2.2 Electrochemical measurements

All electrochemical characterizations were performed by an Autolab PGSTAT101 potentiostat. Cyclic voltammetry was performed in a conventional three-electrode cell. Fluorinated indium tin oxide (FTO) coated glass, with a sheet resistance of 8.1 Ω sq^{-1} (Pilkington), was employed as the working electrode. Before use, the FTO-coated glass was cleaned sequentially in acetone, ethanol, and water using an ultrasonic bath for approximately 10 minutes each, followed by a 3-minute oxygen plasma cleaning. A coiled platinum wire served as the counter electrode, while a silver chloride-coated silver wire (Ag/AgCl) was used as the reference electrode. The Ag/AgCl electrode was prepared galvanostatically in saturated KCl (aq) and calibrated against a ferrocene/ferrocenium (Fc/Fc$^+$) couple, with E_{ref} = 0.45 V in 0.1 M TBAPF$_6$ in acetonitrile. All the potentials are referenced to the Ag/AgCl electrode.

23578 | *J. Mater. Chem. C*, 2025, **13**, 23577–23588

This journal is © The Royal Society of Chemistry 2025

2.3 Electropolymerization

For separate studies, all the polymer films were prepared using 10 and 20 potentiodynamic cycles. For the 20-cycle preparation, 0.04 mM ZnTAPP and/or 0.04 mM EDOT (feed ratio: 1 : 1) were individually added to a 0.1 M TBAPF$_6$ in (DCE : ACN (4 : 1)) solution mixture. For the 10-cycle preparation (intended for *in situ* UV-Vis and EC measurements), 1.2 mM ZnTAPP and/or 1.2 mM EDOT (feed ratio: 1 : 1) were individually added to a 0.1 M TBAPF$_6$ (DCE : ACN (4 : 1)) solution mixture. The electrochemical polymerization was conducted within a potential window of 0.2 and 1.4 V (*vs.* Ag/AgCl) at a scan rate of 20 mV s^{-1}. The resulting thin films were thoroughly rinsed with ACN and DCE, followed by quartz-distilled water, to remove any traces of starting materials from the electrode surfaces. The cleaned films were then stored in a desiccator to preserve their integrity.

2.4 Characterizations

UV-Vis absorption spectra of polymer thin films and individual monomers (dissolved in DCE) were recorded using an Agilent Cary 60 UV-Vis spectrophotometer. Blank FTO was used as a reference for background correction. The CIELAB $L^*a^*b^*$ coordinates represent a uniform color space established by the Commission Internationale de l'Eclairage (CIE) in 1976. In this system, L^* denotes the lightness component, while a^* and b^* correspond to the two opposing chromatic dimensions: red-green and yellow-blue, respectively. These values were calculated using the Cary WINUV color application, employing D50 (5000 K) as the standard illuminant under controlled temperature conditions and a daylight-simulating light source. FTIR spectra of the polymer films were obtained using a Bruker Vertex 70 FTIR spectrometer with an MCT detector cooled with liquid nitrogen. Each spectrum was recorded at 55° incidence angle relative to the surface normal using a Harrick Seagull accessory, compiling 256 scans at 4 cm^{-1} spectral resolution. Raman spectra were recorded by Renishaw inVia confocal Raman microscope equipped with a CCD detector and a Leica microscope. Spectra were recorded with 50× objective, 1800 l mm^{-1} grating using a 532 nm diode laser as the excitation source. XPS measurements of all the polymer thin films on the FTO substrate were recorded by Thermo Scientific Nexsa XPS spectrometer using Al Kα radiation (1486.7 eV). Binding energies were calibrated to the peak position of the main C 1s signal at 284.6 eV of the polyZnTAPP, PEDOT, and poly(ZnTAPP–EDOT). All the XPS spectra were fitted using Avantage with a smart background fitting available in the package. The polymer film surface was analyzed using atomic force microscopy (AFM) conducted by Park systems with a silicon-tipped cantilever operating in non-contact mode. The image processing and analysis were carried out using XEI software. Surface morphology was evaluated using a Thermo Scientific Spreo S field-emission scanning electron microscope (FE-SEM) equipped with an Oxford instrument ultim max 100EDS spectrometer. The contact angles of the polymer thin films were determined under ambient conditions using an Attension Theta optical tensiometer. The measurements were performed with a PC-controlled motorized syringe, ensuring a precision of ±1°. Equilibrium contact angle values were recorded for a 3 μl water droplet dispensed from the syringe needle.

2.5 Theoretical studies

Spin-restricted density functional theory (DFT) based calculations have been performed using the Gaussian 16 software.[35] The electron–electron exchange correlation was approximated using the B3LYP hybrid exchange–correlation functional.[36,37] A LANL2DZ[38–40] basis set was used for the Zn atom and a 6-31G(d) basis for all other types of atoms (C, N, S, O, and H). For Zn, the valence configuration of $4s^23d^{10}$ was utilized, while for other atoms, all electrons have been included in the calculation. Additionally, the empirical dispersion correction GD3 was incorporated.[41] For the EDOT ligands, the B3LYP hybrid exchange–correlation functional was employed with 6-31G(d) basis functions. Frequency analysis was conducted for all optimized structures to evaluate the stability of all possible configurations. Molecular orbitals of all the configurations using VESTA software.[42] Absorption spectra were computed using the TDDFT approach using the hybrid B3LYP and cam-B3LYP functionals, and the wave functions were expanded with a 6-311g(d) basis set for C, H, S, N, and O atoms. For the Zn atom, the LANL2DZ basis set was used, and the GD3 dispersion correction was incorporated.

2.6 *In situ* UV-Vis and electrochromic studies

Experiments were conducted in a quartz cuvette of path length 1 cm, with FTO as a working electrode, Pt wire as a counter electrode, and Ag/AgCl as a quasi-reference electrode. UV-Vis spectra were recorded by an Agilent Cary 60 UV-Vis spectrophotometer with blank FTO serving as the reference for background correction. The cell was connected to an Autolab PGSTAT101 potentiostat. Spectra were recorded in the potential range of −0.5 to +0.5 V, with potential adjustments made in 100 mV intervals in potentiostatic mode. The switching response was recorded for 200 cycles at selected wavelengths with a potential of −0. 5 V to +0.5 V and a time interval of 20 s. The EC studies were performed by switching the potential between −0.5 V to +0.5 V.

3. Results and discussion

The progression of polymer growth during electropolymerization is evidenced by the increasing peak current intensity observed in cyclic voltammetry (CV) scans (Fig. 1). Fig. 1(a) and (b) present the cyclic voltammetry (CV) plots of the electropolymerization of EDOT and ZnTAPP, respectively. The formation of a blue film ($L^* = 84.14$, $a^* = −4.83$, $b^* = −3.24$) on the electrode surface (Fig. 2(a), inset) confirms the formation of PEDOT. Similarly, the appearance of brown film ($L^* = 75.70$, $a^* = 2.11$, $b^* = 26.68$) on the electrode surface (Fig. 2(b), inset) indicates the successful polymerization of ZnTAPP to poly-ZnTAPP. The CV profile for EDOT polymerization (Fig. 1(a) and (d)) aligns well with previously reported data.[43] In the case of ZnTAPP (Fig. 1(b) and (e)), the first scan displays reversible

This journal is © The Royal Society of Chemistry 2025

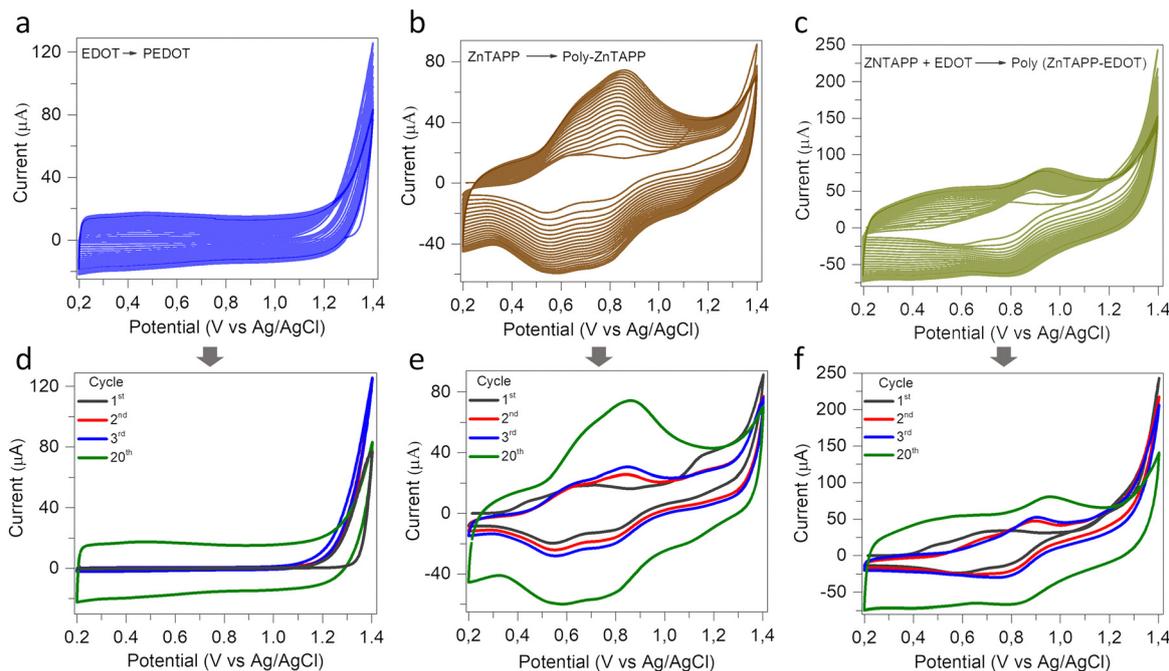*J. Mater. Chem. C*, 2025, **13**, 23577–23588 | **23579**

Fig. 1 Electropolymerization of (CV plots at a scan rate of 20 mV s^{-1}) (a) EDOT to PEDOT, (b) ZnTAPP to polyZNTAPP, and (c) ZnTAPP + EDOT to poly(ZnTAPP–EDOT), and their respective (d)–(f) 1st, 2nd, 3rd and 20th CV plots in DCE : ACN (4 : 1) containing 0.1 M TBAPF$_6$ swept between 0.2 to 1.4 V *vs.* Ag/AgCl at a scan rate of 20 mV s^{-1}.

oxidation and reduction peaks at $\sim$0.65 V and $\sim$0.54 V, respectively, attributed to the amino substituents on the porphyrin ring.[25,44] Additionally, an oxidation peak is observed at $\sim$0.43 V, which can be associated with adsorbed species.[45] Another oxidation peak appears at $\sim$1.14 V during the initial scan; however, both peaks are absent in the following cycles.[32,45,46] A reduction peak at $\sim$0.8 V appears during the reverse scan. From the second CV scan onward, well-defined reversible oxidation/reduction peaks emerge at $\sim$0.63/0.56 V and $\sim$0.83/0.8 V, indicating the formation of an electroactive film. When the applied potential remains below the oxidation threshold of the porphyrin ring, the polymerization primarily proceeds through the oxidation of amino groups, possibly forming dihydrophenazine and/or phenazine linkages[25,47] (Scheme S2). Notably, the CV profile recorded during the electrocopolymerization of ZnTAPP–EDOT exhibits characteristics of both monomers. In the first cycle, irreversible peaks appear at $\sim$0.47 V and $\sim$1.18 V, similar to those observed in ZnTAPP polymerization, accompanied by two cathodic peaks at around 0.81 V and 0.57 V. From the second cycle onward, prominent redox peaks observed at $\sim$0.89 V (oxidation) and $\sim$0.78 V (reduction), shifting gradually to $\sim$0.95 V and $\sim$0.83 V after 20 cycles. This evolution corresponds to the growth of a uniform, electroactive poly(ZnTAPP–EDOT) film with a dark green color ($L^* = 72.11$, $a^* = -3.14$, $b^* = 23.39$). The electropolymerization process is initiated by the oxidation of monomer units, leading to the formation of radical cations that couple to form polymer chains. However, the exact sequence and spatial arrangement of monomer units within the resulting copolymer remain unclear. The detailed propagation mechanism is still

not fully understood, though current evidence suggests that copolymerization likely proceeds *via* amino-α coupling (see SI).

Fig. 2 shows the SEM and AFM images of PEDOT, polyZnTAPP, and poly(ZnTAPP–EDOT) thin films. All film surfaces displayed uniform morphology. SEM images revealed that PEDOT formed an interconnected web of nanofibers with an average diameter of 24 nm. In contrast, polyZnTAPP exhibited a compact globular morphology with an average globule diameter of 183 nm. Notably, SEM images of poly(ZnTAPP–EDOT) revealed a distinct flower-like architecture with an average structural diameter of approximately 207 nm. The copolymer structure also showed slight porosity, which is likely to facilitate ion diffusion and migration during the electrochemical process.[20] AFM images corroborated the SEM findings, confirming the uniformity of all polymer films. Film thickness and surface profiles were analyzed using AFM in non-contact mode. After 20 electropolymerization cycles, the average thicknesses of PEDOT, polyZnTAPP, and poly(ZnTAPP–EDOT) films were measured as 86.5 nm, 38.1 nm, and 110.1 nm, respectively. The root mean square (RMS) surface roughness was evaluated over a 5×5 μm^2 area. The RMS roughness values were approximately 102.4 nm for PEDOT, 11.6 nm for polyZnTAPP, and 10.2 nm for poly(ZnTAPP–EDOT). To evaluate surface wettability, the water contact angle (CA) of all polymer films was measured (Fig. 2(a)–(c), insets). A reduction in hydrophilicity was observed for the poly(ZnTAPP–EDOT) copolymer (CA = 40°) compared to PEDOT (CA = 24°) and polyZnTAPP (CA = 36°), indicating a modification in surface properties.

The UV-Vis spectrum of the poly(ZnTAPP–EDOT) film (Fig. 3(a)) showed the combined spectral features of both monomers (also in SI). The broadened absorption bands at
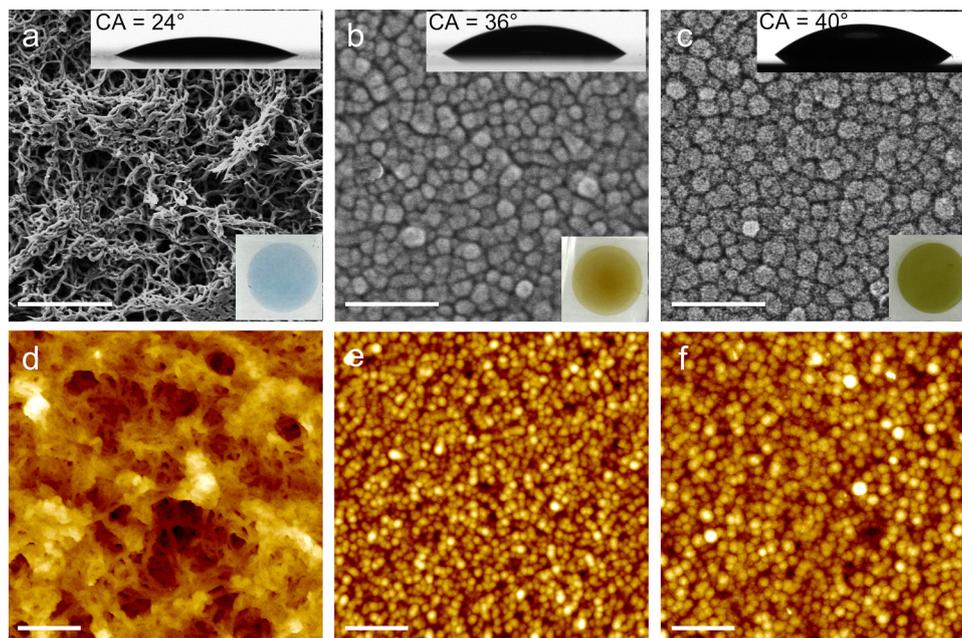
23580 | *J. Mater. Chem. C*, 2025, **13**, 23577–23588

This journal is © The Royal Society of Chemistry 2025

Fig. 2 SEM images of (a) PEDOT, (b) polyZnTAPP, and (c) poly(ZnTAPP–EDOT) and AFM images of (d) PEDOT, (e) polyZnTAPP, and (f) poly(ZnTAPP–EDOT). (a)–(f) scale = 1 μm. Insets in (a)–(c) show the water contact angle and color of the polymer films.

lower wavelengths, along with the broad shoulder in the higher-wavelength region extending into the bNIR, are characteristic of porphyrin and PEDOT, respectively. These features indicate the presence of a conjugated network and extensive electronic delocalization in the poly(ZnTAPP–EDOT) copolymer.[32,48]

The FTIR and Raman spectra of the polymer thin films revealed all characteristic peaks, as shown in Fig. 3(b) and (c) (details in Tables S2–S5). For poly(ZnTAPP–EDOT), the presence of stretching peaks corresponding to both EDOT and porphyrin units confirmed the successful formation of the copolymer. The C–S–C stretching peak of the EDOT unit appeared at 825 cm^{-1}. Additionally, peaks at around 1070 cm^{-1} and 1137 cm^{-1} were attributed to the stretching vibrations of the alkylene deoxy group in EDOT (Table S2).[49,50] Peaks at 968 cm^{-1} and 1012 cm^{-1} are characteristic of pyrrole ring deformation and Zn–N coordination within the porphyrin core,[51] indicating retention of the porphyrin backbone during the copolymerization. The N–H stretching vibrations (3360–3500 cm^{-1}) of the amino groups appeared slightly broadened and redshifted, suggesting interactions during copolymerization.[25,51] However, not all amino groups participated in the reaction. The absence of characteristic phenazine bands in poly(ZnTAPP–EDOT) confirmed that the copolymerization produced EC polymer networks instead of phenazine-type linkages (Table S3).[25] Raman spectroscopy revealed numerous active modes for the copolymer poly(ZnTAPP–EDOT) (Tables S4 and S5). The characteristic bands at 440 cm^{-1}, 577 cm^{-1}, and 988 cm^{-1} were assigned to oxyethylene ring deformation. The 703 cm^{-1} band corresponded to symmetric C–S–C deformation. Vibrations at 1367 cm^{-1} and 1567 cm^{-1} were assigned to C–C stretching and asymmetric $C_{\alpha}{=}C_{\beta}$ vibrations from the EDOT units.[49,50,52] Peaks attributed to ZnTAPP unit included bands at 411 cm^{-1} (Zn–N stretch and pyrrole ring deformation), 664 cm^{-1} (related to C_{β}–H

non-plane bending), and a series of in-plane bending vibrations at 885 cm^{-1}, 1013 cm^{-1}, 1068 cm^{-1}, 1183 cm^{-1}, and 1243 cm^{-1} (associated with C_m–C_{ph}, C_{β}–H, and C_{ph}–H). Additional peaks at 1353 cm^{-1} (C–N bonds in the pyrrole ring), 1458 cm^{-1} (C_{β}–C_{β} and C_m–C_{ph}), and 1541 cm^{-1} (asymmetric stretching and bending deformation of the C_{α}–C_m–C_{α}), further confirmed ZnTAPP incorporation into the copolymer.[53]

Surface chemical analysis of polymer films was investigated by XPS. The XPS spectra of PEDOT and polyZnTAPP are discussed in (Fig. S5 and S6).[51,54–56] For poly(ZnTAPP–EDOT), significant features were observed in the C 1s, N 1s, S 2p, O 1s, and Zn 2p spectra (Fig. 3(d)–(i)). The C 1s spectra were deconvoluted into five peaks located at 284.6 eV (C–C/C=C), 285.8 eV (C–N), 286.7 eV (C–S), 287.5 eV (C=C–O), and 288.3 eV (C=N) binding energies (BEs). Shake-up satellite peaks at around 288.6 eV and 291.2 eV, originating from adventitious carbon. The N 1s spectrum displayed features typical of porphyrin systems, 398.2 eV (Zn–N binding), 399.3 eV (aprotic pyrrolic N), 400.3 eV (imine linkers N), and 402.0 eV (amine N in phenyl groups), with a satellite component at higher BE.[51] The S 2p spectrum exhibited a well-resolved spin–orbit doublet at 164.0 eV and 165.2 eV (Δ = 1.2 eV), consistent with thiophene sulphur in EDOT.[54,56] At high BE, a broad tail indicated π-electron delocalization. The O 1s spectrum showed distinct peaks at 532.0 eV and 533.4 eV, corresponding to C–O–C and C–O bonds. From the Zn 2p spectrum, peaks at 1021.3 eV (Zn $2p_{3/2}$) and 1044.4 eV (Zn $2p_{1/2}$) confirmed the presence of Zn(II) in the copolymer.[55] F 1s and P 2p peaks were attributed to hexafluorophosphate counterions, present in all polymer matrices.[57] While XPS peak intensities broadly agreed with elemental composition, accurately correlating them to atomic percentages remains challenging. The average surface composition derived from XPS gave
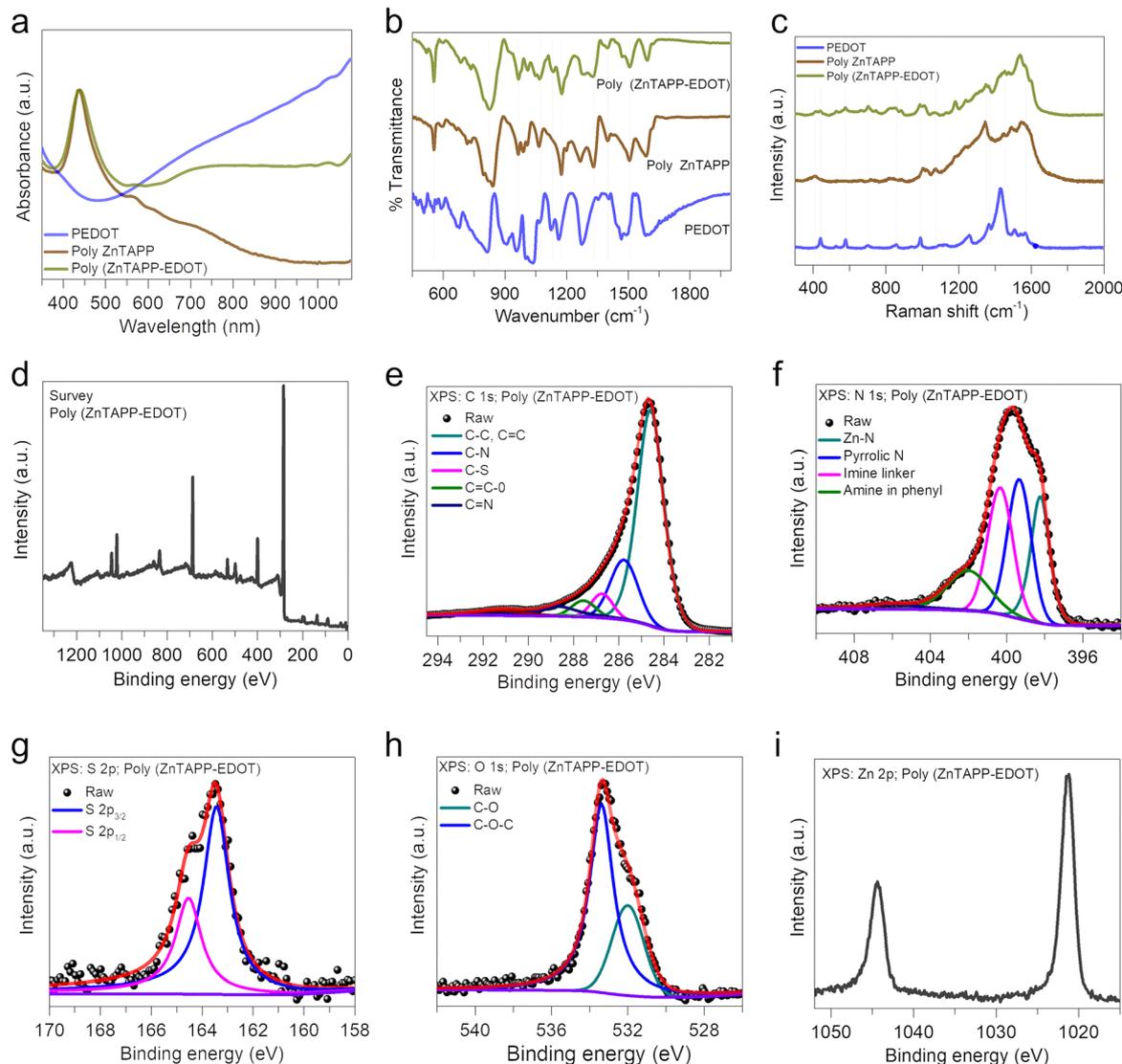
This journal is © The Royal Society of Chemistry 2025

J. Mater. Chem. C, 2025, **13**, 23577–23588 | **23581**

Fig. 3 (a) UV-Vis, (b) FTIR, and (c) Raman spectra of PEDOT, polyZNTAPP, and poly(ZnTAPP–EDOT). (d) XPS survey (e) C 1s, (f) N 1s, (g) S 2p, (h) O 1s, and (i) Zn 2p XPS plots of poly(ZnTAPP–EDOT).

Zn/S and Zn/N atomic ratios of approximately 1:1 and 1:9, respectively. The slight deviation in the Zn/N ratio is likely due to surface enrichment of nitrogen-containing electrolytes. We propose that the copolymerization follows a specific sequence, rather than proceeding through alternating sequences, resulting in distinct EC behavior (Scheme S3).

TDDFT data on ZnTAPP–(EDOT)$_1$–ZnTAPP, ZnTAPP–(EDOT)$_2$–ZnTAPP, and ZnTAPP–(EDOT)$_3$–ZnTAPP are shown in Fig. 4 and Table 1. We stepwise increased the number of EDOT linkers between the two ZnTAPP units to gain better insights into the experimental observations of poly(ZnTAPP–EDOT). A minimal shift in the low-intensity Q-band peaks (ZnTAPP–(EDOT)$_1$–ZnTAPP – 561 nm, ZnTAPP–(EDOT)$_2$–ZnTAPP – 561.9 nm, and ZnTAPP–(EDOT)$_3$–ZnTAPP – 562.9 nm) was observed as EDOT content was increased from 1–3. Interestingly, these peaks exhibited a significant ~ 67 nm blue shift compared to the Q-bands of the ZnTAPP trimer, highlighting the electronic impact of the EDOT linkage. In the Soret region, ZnTAPP–

(EDOT)$_1$–ZnTAPP showed a dominant transition at 409.8 nm (oscillator strength: 1.27), driven by H−10 → L (13%) and H−3 → L+1 (23%). For ZnTAPP–(EDOT)$_2$–ZnTAPP, this band redshifted to 414.7 nm (oscillator strength: 1.66) with key contributions from H−5 → L+3 (14%) and H−3 → L+2 (12%). Notably, ZnTAPP–(EDOT)$_3$–ZnTAPP exhibited a pronounced redshift of the Soret band to 443.8 nm with a significantly higher oscillator strength of 2.35, mainly driven by the H → L+4 (75%) transition. These results indicate that increasing EDOT linkage enhances electron delocalization and strengthens optical absorption, with ZnTAPP–(EDOT)$_3$–ZnTAPP showing the most pronounced shift. To further confirm these observations, TDDFT simulations were performed for EDOT–ZnTAPP–EDOT–ZnTAPP. The resulting spectra closely matched those of ZnTAPP–EDOT–ZnTAPP, reinforcing the conclusion that EDOT's position and quantity play a decisive role in shaping the optical features of the copolymer. Overall, these findings demonstrate that the electronic and optical properties of ZnTAPP-based systems are highly
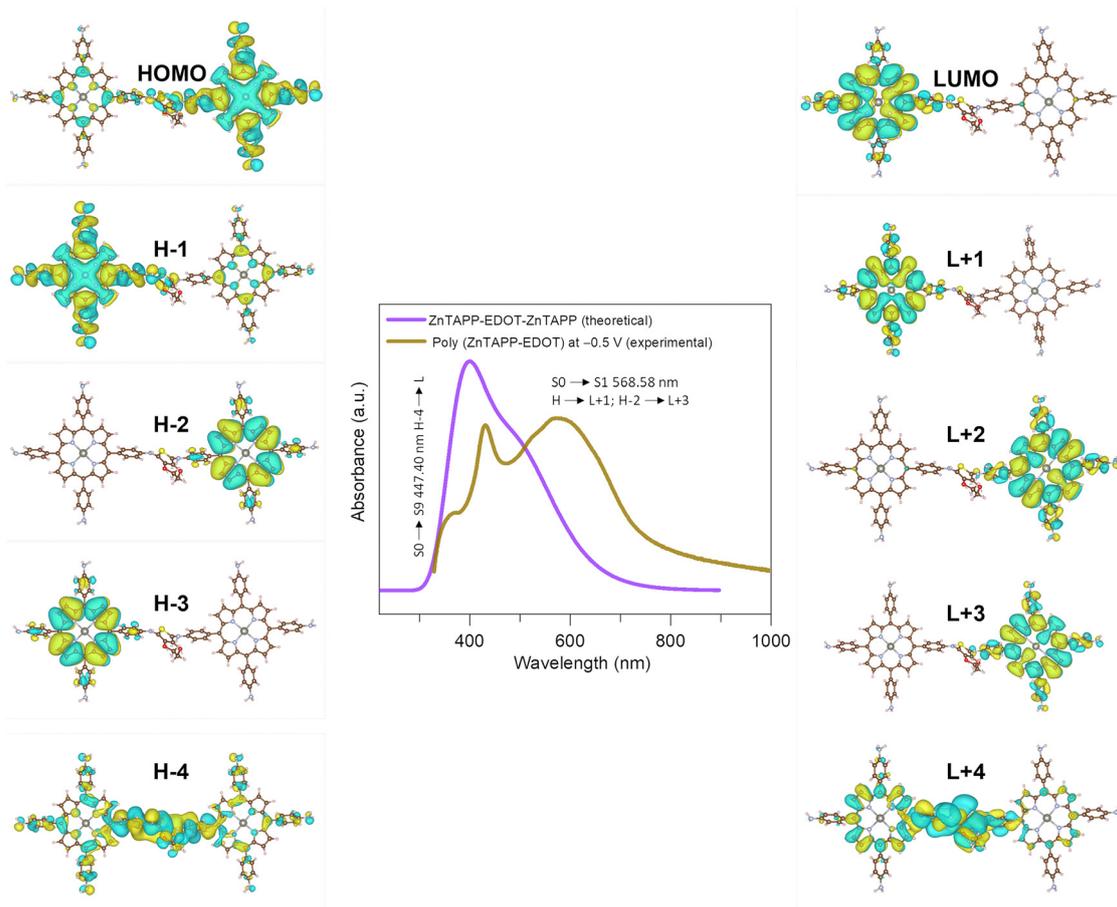
23582 | *J. Mater. Chem. C*, 2025, **13**, 23577–23588

This journal is © The Royal Society of Chemistry 2025

Fig. 4 Comparison of computed spectra of ZnTAPP–(EDOT)$_n$–ZnTAPP (n = 1, 2, and 3) along with ZnTAPP–EDOT–ZnTAPP–EDOT and the molecular orbitals of ZnTAPP–(EDOT)$_3$–ZnTAPP (HOMO: highest occupied molecular orbital and LUMO: lowest occupied molecular orbital, isocounter: 0.01) involved in the transitions.

Table 1 The important TDDFT major electronic transitions and oscillator strengths of ZnTAPP–(EDOT)$_n$–ZnTAPP (n = 1, 2, and 3) and EDOT–ZnTAPP–EDOT–ZnTAPP

Wavelength (nm)	Oscillator strength	Major transitions							
ZnTAPP–(EDOT)$_1$–ZnTAPP									
561.12	0.1206	H−3 → L+1	24%	H−1 → LUMO	31%	HOMO → LUMO	22%		
411.88	0.898	H−10 → LUMO	13%	H−7 → L+1	11%	H−6 → LUMO	10%	H−3 → L+1	23%
409.78	1.2713	H−3 → LUMO	12%	H−2 → L+2	16%	H−11 → L+1	4%	H−11 → L+3	8%
409.35	0.1963	H−6 → LUMO	13%	H−5 → L+2	21%				
ZnTAPP–(EDOT)$_2$–ZnTAPP									
561.83	0.1299	H−4 → LUMO	22%	H−1 → L+1	32%	HOMO → L+1	18%		
414.69	1.6584	H−5 → L+3	14%	H−3 → L+2	12%	H−3 → L+3	11%	H−12 → L+1	2%
410.72	0.4615	H−11 → L+2	11%	H−6 → L+2	14%	H−3 → L+3	15%		
409.88	0.6212	H−4 → L+1	13%	H−12 → LUMO	8%				
409.41	0.5035	H−7 → LUMO	10%	H−4 → LUMO	15%	H−4 → L+1	10%		
ZnTAPP–(EDOT)$_3$–ZnTAPP									
562.93	0.204	H−1 → L+3	14%	H−4 → LUMO	9%	H−4 → L+2	5%	H−3 → L+1	7%
443.75	2.3516	HOMO → L+4	75%						
ZnTAPP–EDOT–ZnTAPP–EDOT									
561.62	0.1326	HOMO → LUMO	26.7%	H−1 → LUMO	23.3%	H−3 → L+1	22.7%		
444.68	0.3056	H−4 → L	58.3%	H−4 → L+1	22.9%				
419.6	0.5515	H−5 → L	41.5%	H−5 → L+1	21.1%				
410.08	0.5608	H−2 → L+2	13.3%	H−5 → L+1	11.6%	H−2 → L+3	11.6%		

This journal is © The Royal Society of Chemistry 2025

J. Mater. Chem. C, 2025, **13**, 23577–23588 | **23583**

sensitive to the structural arrangement and delocalization effects of EDOT units. This underscores the importance of molecular design in tailoring materials for enhanced optoelectronic performance. Frontier molecular orbitals associated with these transitions are provided in Tables S6 and S7 (see also Fig. S7 for visualization). The TDDFT predicted UV-vis spectra for $ZnTAPP_3$ offer insight into their electronic properties and show strong agreement with experimental data (Fig. S8a and Table S8). Additionally, TDDFT spectra were calculated for $EDOT_n$ ($n = 1–4$) in their neutral forms to support the interpretation of results (Fig. S8b).

Based on TDDFT simulations, electropolymerization behavior, and analysis, we propose a plausible mechanistic pathway for the electrocopolymerization of ZnTAPP and EDOT (Scheme S3). The Zn:S atomic ratio observed in XPS suggests a balanced incorporation of both monomer units within the copolymer matrix. Given the similar oxidation potentials of ZnTAPP and EDOT, it is likely that both monomers undergo oxidation simultaneously on the FTO electrode surface, generating radical cations that subsequently couple to form the copolymer network. This simultaneous oxidation and coupling mechanism aligns with previous studies on electrocopolymerization of monomeric mixtures, where the oxidation potentials of the monomers play a crucial role in determining the copolymer structure.[58] To confirm this, individual electropolymerization of each monomer was performed (Fig. 1(a) and (b)), verifying their oxidation behavior and supporting their compatibility for copolymerization. Under electrochemical conditions, such radical coupling is more likely to result in a specific sequence of copolymer rather than an alternating one.[59] Considering the steric bulk of the ZnTAPP unit and the TDDFT results, the polymerization likely follows a pathway where multiple EDOT units bridge adjacent ZnTAPP moieties. This is consistent with the observed polaronic features in the copolymer and the TDDFT-predicted preference for at least three EDOT units between ZnTAPP units.[60,61] Such an arrangement supports effective π-delocalization and accounts for the structural and optical behavior of the final copolymer, which likely contains a varied sequence distribution with a balanced representation of both monomeric components.

The electronic structure and optical properties of the polymer films were evaluated using operando UV-Vis spectroscopy. Fig. 5 shows the absorption spectra of the polymer films at various applied potentials, spanning the visible to bNIR region. PEDOT exhibited a broad and intense absorption peak centered around 608 nm, corresponding to the π–π^* transition in its neutral state (at -0.5 V), resulting in a deep blue film ($L^* = 28.34$, $a^* = 7.96$, $b^* = -43.01$). As the potential increased from -0.5 V to $+0.5$ V, the formation of polarons was evidenced by a gradual decrease in the 608 nm peak and the growth of a broad absorption band around 800 nm, extending into the bNIR through a well-defined isosbestic point.[62,63] At higher positive potentials ($+0.5$ V), a new band emerged at approximately 950–1000 nm, attributed to bipolaron formation in PEDOT ($L^* = 65.25$, $a^* = -9.83$, $b^* = -18.76$).[64] In contrast, polyZnTAPP films showed minimal electrochromic response across the applied potential range (-0.5 V to $+0.5$ V) (Fig. 5(b)). The colorimetric values remained relatively constant ($L^* = 75.61$, $a^* = 0.75$, $b^* = 33.11$ at -0.5 V and $L^* = 74.72$, $a^* = 0.47$, $b^* = 31.69$ at $+0.5$ V). Upon oxidation, only a slight reduction in the Soret band (430 nm) intensity and a minor increase in the Q bands (565 nm and 610 nm) were observed, along with the emergence of a weak band around 685 nm.[15]

The poly(ZnTAPP–EDOT) copolymer exhibited spectral features of both ZnTAPP and EDOT units (Fig. 4(c)). At -0.5 V ($L^* = 54.70$, $a^* = -1.84$, $b^* = -6.67$), the orange brown copolymer showed a distinct Soret band at ~ 430 nm and a Q band at ~ 523 nm. A second Q band at ~ 564 nm overlapped with PEDOT's absorption at ~ 575 nm, which became more prominent at higher potentials. A hypsochromic shift (blue shift) of approximately 44 nm in the Q bands was observed, suggesting a higher degree of polymerization and influence of EDOT units in the copolymer network (Fig. 5(c)). Upon oxidation, the intensity of the porphyrin bands gradually decreased, while a broad absorption band developed around 750 nm, extending into the bNIR, again passing through a clear isosbestic point. These features indicate the formation of polaron-like structures in the copolymer backbone,[63] facilitating π electrons migration between at least 3 EDOT units and porphyrin in the copolymer network.[60,61] The absorption at ~ 575 nm, corresponding to the π–π^* transition, progressively diminished during oxidation. While at $+0.5$ V, an olive green copolymer film with bipolaron band appeared above 900 nm
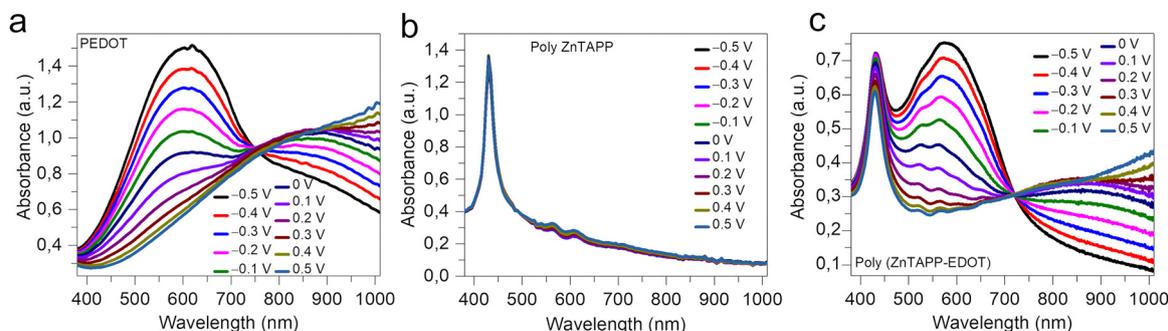

Fig. 5 *In situ* UV-Vis spectra of the (a) PEDOT, (b) polyZnTAPP, and (c) poly(ZnTAPP–EDOT) film deposited on FTO electrode in 0.1 M $TBAPF_6$ in ACN with Ag/AgCl as reference electrode and Pt wire as the counter electrode.

23584 | *J. Mater. Chem. C*, 2025, **13**, 23577–23588

This journal is © The Royal Society of Chemistry 2025

due to π-polaron transition ($L^* = 74.72$, $a^* = 0.47$, $b^* = 14.52$). These results confirm the integration of monomeric and oligomeric EDOT and ZnTAPP units in the polymer backbone, significantly influencing the electrochromic and optical behavior of the copolymer. A detailed comparison of the forward and reverse scans is provided in Fig. S11.[65] Importantly, the potential range associated with the main spectral transitions closely aligns with the redox peaks observed in the cyclic voltammogram (Fig. S2a), supporting the electrochemical origin of these optical changes.

Kinetic studies were conducted to evaluate the electrochromic characteristics of the copolymer. Potentials were applied to switch the film between its neutral state (-0.5 V) and oxidized state ($+0.5$ V), with percentage transmittance monitored at specific wavelengths during potential switching every 20 s. Fig. 6 illustrates the variation in transmittance in response to the applied potentials at 575 nm and 1020 nm. The switching time refers to the speed at which an electrochemical system changes from one redox state to another when an external potential is applied.

The copolymer film exhibited rapid switching behavior, attributed to its high ion diffusion rate. At an applied potential of -0.5 V, the copolymer actively blocked visible light, and at $+0.5$ V, it blocked bNIR light. The copolymer showed an optical contrast of 25% at 575 nm and 31% at 1020 nm (Fig. 6(a) and (d)) upon switching between ± 0.5 V and *vice versa*, respectively. In contrast, poly(ZnTAPP) did not exhibit electrochromic activity (Fig. S12a). The transition from the neutral to 90% oxidized state occurred within 0.36 s and 0.65 s at 575 nm and 1020 nm, respectively. The reverse transition required 0.67 s and 1.8 s for the respective wavelengths, confirming a notably fast response (<2 s) for a 1.2 cm^2 copolymer film. The copolymerization of ZnTAPP with EDOT enhanced the visible–bNIR EC performance. Poly(ZnTAPP–EDOT) retains 88% and 82% of its EC performance after 200 redox (8000 s) cycles in the visible (@575 nm) and bNIR (@1020 nm) regions, respectively (Fig. 6(b) and (e)). Even after 16 000 s (400 cycles), the poly(ZnTAPP–EDOT) film retained excellent stability, along with a visibly apparent color change (Fig. S13).[27] Comparatively, PEDOT exhibits lower optical contrasts of 15% in the bNIR region at 1020 nm and 24% at 608 nm. In addition, PEDOT shows longer coloration times.

The coloring efficiency (CE) (η) of the system is defined as the proportion of the change in optical density (ΔOD) and the quantity of electronic charge (Q) injected or ejected into the system (polymer film) per unit area. It reflects the energy efficiency of the EC material. The relationship between ΔOD and the transmittance values in the oxidized (T_o) and neutral (T_n) states is expressed as: ΔOD $= \log(T_o/T_n)$. The η values for the poly(ZnTAPP–EDOT) are 434 cm^2 C^{-1}@575 nm and 182 cm^2 C^{-1}@1020 nm, which were obtained from the slope of ΔOD *vs.* Q curves (Fig. S14). The CE of poly(ZnTAPP–EDOT) was comparable to that of PEDOT (Table S12). This enhancement is attributed to the synergistic interaction between ZnTAPP and EDOT, which promotes efficient counterion transport within the copolymer matrix. As a result, smaller charge injection is sufficient to induce a significant optical change, yielding higher contrast ratios and energy-efficient switching behavior. This makes the copolymer suitable for practical applications.

Optical memory, also known as open circuit memory, refers to the ability of EC materials to retain their optical state after the electric field is removed, a property essential for energy-efficient EC materials.[66,67] The optical spectra for Poly(ZnTAPP–EDOT) were recorded at 575 nm and 1020 nm as a function of time by alternately applying potentials of ± 0.5 V for 2 s with a
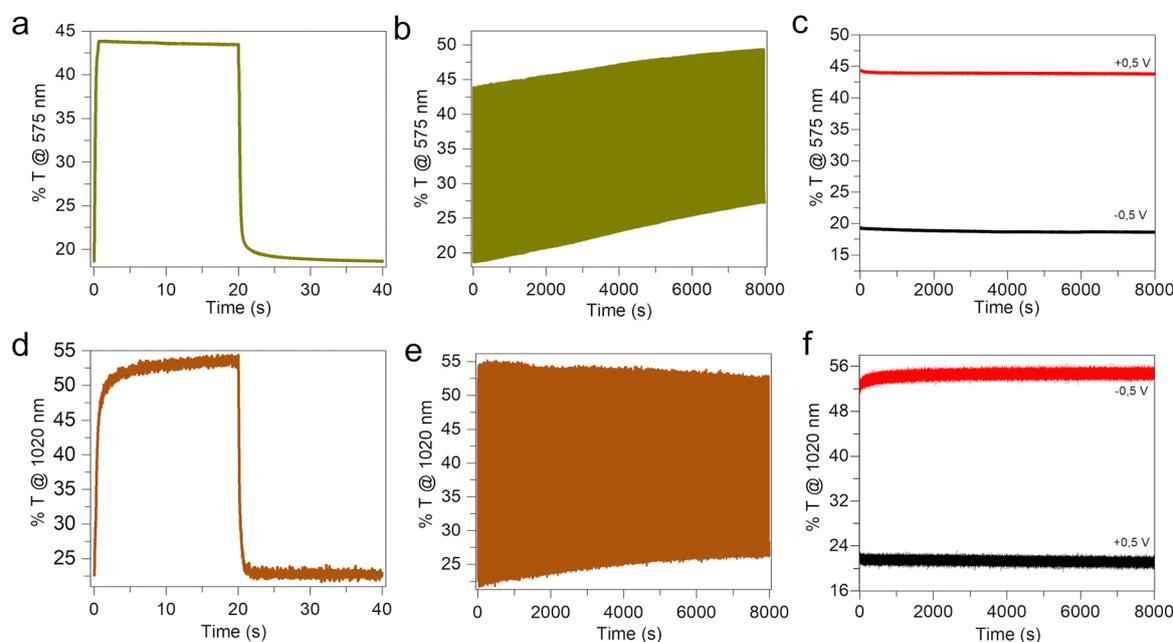

Fig. 6 Electrochromic switching data for the poly(ZnTAPP–EDOT) (a) and (d) 1st cycle, (b) and (e) 200 cycles, and (c) and (f) optical memory at 575 nm and 1020 nm, respectively.

200 s open circuit interval. As shown in Fig. 6(c) and (f), the transmittance values exhibited negligible change over 8000 s in the copolymer film, demonstrating excellent optical memory under open-circuit conditions. These findings affirm the material's potential for use in energy-efficient EC devices (ECDs).

Electrochemical impedance spectroscopy (Fig. S15) was performed to understand the equivalent series resistance (ESR) and charge transfer resistance (R_{CT}) of PEDOT, polyZnTAPP, and poly(ZnTAPP–EDOT). The semicircle in the Nyquist plot is characteristic of the kinetic processes in the film (characterized by the R_{CT}), indicative of the doping/dedoping process. A semicircle was observed with both PEDOT and poly(ZnTAPP–EDOT) thin films, suggesting a doping/dedoping phenomenon. However, the poly(ZnTAPP–EDOT) thin film showed a larger R_{CT}, indicating sluggish kinetics. In contrast, the absence of a semicircle in the polyZnTAPP film indicates high resistance and a non-doping nature. In the low-frequency region, both PEDOT and poly(ZnTAPP–EDOT) films exhibited a nearly vertical profile, characteristic of capacitive behavior, whereas the polyZnTAPP film deviated from this trend. These observations suggest that PEDOT and poly(ZnTAPP–EDOT) possess significantly higher capacitance, enhancing their electrochemical performance relative to polyZnTAPP.[44]

4. Conclusion

We have successfully synthesized and characterized an electrochromic copolymer thin film of poly(ZnTAPP–EDOT) *via* electropolymerization. Cyclic voltammetry revealed that polymerization proceeds through radical cation formation followed by coupling reactions. The resulting copolymer demonstrated a distinct flower-like morphology and exhibited reversible color changes (orange brown to olive green) upon applying potential. The color changes lead to strong absorption in the Vis (π–π^* transition) and bNIR regions (due to polaron formation). The copolymer showed fast switching and good coloring efficiency in the Visible and bNIR region on applying ± 0.5 V *versus* Ag/Ag$^+$. The films showed optical contrast of 25% and 31% at 575 nm and 1020 nm, respectively, with strong EC memory and stability over multiple redox cycles, inferring that the electrocopolymerization of ZnTAPP with EDOT can enhance the Vis–bNIR electrochromism. Additionally, copolymerization enables access to new hues, expanding the color palette of EC materials.

TDDFT calculations on ZnTAPP–(EDOT)$_1$–ZnTAPP, ZnTAPP–(EDOT)$_2$–ZnTAPP, and ZnTAPP–(EDOT)$_3$–ZnTAPP revealed a systematic redshift in absorption bands with increasing EDOT linkages, driven by $\pi \rightarrow \pi^*$ transitions localized on the ZnTAPP units. These findings support a mechanistic pathway involving simultaneous oxidation of both monomers and a preference for multiple EDOT bridges between porphyrin units, favoring a specific sequence in copolymer structure. This mechanism is consistent with previous studies on multichromic copolymers, where oxidation potential alignment and steric effects govern sequence distribution.

This work establishes a mechanistic and foundational framework for designing porphyrin–EDOT systems with improved optical and electronic features. The electropolymerization approach can be extended to other functional porphyrin derivatives, alternative metal centers, mixed metal centers, and various classes of organic molecules, offering a robust strategy for developing tunable EC devices.

Author contributions

Sachin Kochrekar: writing – original draft, visualization, methodology, investigation, formal analysis, funding acquisition, conceptualization. Subrahmanyam Sappati: writing – review & editing, investigation, methodology, formal analysis. Plawan Kumar Jha: writing – original draft, visualization, supervision, formal analysis. Ermei Mäkilä: formal analysis. Ashwini Jadhav: writing – review & editing, formal analysis. Pia Damlin: writing – review & editing, supervision. Mikko Salomäki: writing – review & editing, formal analysis. Carita Kvarnström: writing – review & editing, supervision, resources, project administration.

Conflicts of interest

There are no conflicts to declare.

Data availability

All measurement data (laboratory notebooks, shared electronic notebooks, raw data files from experiments, experimental analysis data files, and microscopy images) will be located in automatically backed-up servers at UTU. The research data is later deposited within the IDA repository of CSC to ensure that the research community has long-term access to the data.

The data supporting this article have been included as part of the supplementary information (SI). Supplementary information is available. See DOI: **https://doi.org/10.1039/d5tc03045e**.

Acknowledgements

References

1 A. Kumar, L. T. Williams, A. C. Martin, E. Mäkilä, A. M. Figueroa-Navedo and D. F. Leila, *ACS Appl. Mater. Interfaces*, 2018, **10**, 43177–43183.

2 Y. Ji, C. Qin, H. Niu, L. Sun, Z. Jin and X. Bai, *Dyes Pigm.*, 2015, **117**, 72–82.

3 W. Zhang, H. Li, E. Hopmann and A. Y. Elezzabi, *Nanophotonics*, 2020, **10**, 825–850.

4 R. J. Mortimer, *Chem. Soc. Rev.*, 1997, **26**, 147–156.

5 C. G. Granqvist, M. A. Arvizu, B. Pehlivan, H. Y. Qu, R. T. Wen and G. A. Niklasson, *Electrochim. Acta*, 2018, **259**, 1170–1182.

6 J. R. Platt, *J. Chem. Phys.*, 1961, **34**, 862–863.

7 R. J. Mortimer, A. L. Dyer and J. R. Reynolds, *Displays*, 2006, **27**, 2–18.

8 C. Jiang, R. Ge, C. Bian, L. Chen, X. Wang, Y. Zheng, G. Xu, G. Cai and X. Xiao, *Nanoscale*, 2023, **15**, 15450–15471.

9 C. Kortz, A. Hein, M. Ciobanu, L. Walder and E. Oesterschulze, *Nat. Commun.*, 2019, **10**, 4874–4881.

10 Q. Du, Y. Wei, J. Zheng and C. Xu, *Electrochim. Acta*, 2014, **132**, 258–264.

11 G. Sonmez, *Chem. Commun.*, 2005, **42**, 5251–5259.

12 H. Niu, H. Kang, J. Cai, C. Wang, X. Bai and W. Wang, *Polym. Chem.*, 2011, **2**, 2804–2817.

13 A. A. Argun, P. H. Aubert, B. C. Thompson, I. Schwendeman, C. L. Gaupp, J. Hwang, N. J. Pinto, D. B. Tanner, A. G. MacDiarmid and J. R. Reynolds, *Chem. Mater.*, 2004, **16**, 4401–4412.

14 H. Yue, X. Guo, Y. Du, Y. Zhang, H. Du, J. Zhao and J. Zhang, *Synth. Met.*, 2021, **271**, 116619.

15 Y. Guo, X. Hao, Y. Tao, C. Zhang and H. Cheng, *Synth. Met.*, 2019, **258**, 116202.

16 H. Ma, Y. Chen, X. Li and B. Li, *Adv. Funct. Mater.*, 2021, **31**, 2101861.

17 T. Tabak, S. Altinisik, S. Ulucay, S. Koyuncu and K. Kaya, *Macromolecules*, 2024, **57**, 4769–4781.

18 B. C. Thompson, P. Schottland, K. Zong and J. R. Reynolds, *Chem. Mater.*, 2000, **12**, 1563–1571.

19 A. A. Argun, P. H. Aubert, B. C. Thompson, I. Schwendeman, C. L. Gaupp, J. Hwang, N. J. Pinto, D. B. Tanner, A. G. MacDiarmid and J. R. Reynolds, *Chem. Mater.*, 2004, **16**, 4401–4412.

20 C. Gu, A. B. Jia, Y. M. Zhang and S. X. A. Zhang, *Chem. Rev.*, 2022, **122**, 14679–14721.

21 B. B. Carbas, S. Özbakır and Y. Kaya, *Synth. Met.*, 2023, **293**, 117298.

22 J. E. Durantini, R. Rubio, C. Solis, L. Macor, G. M. Morales, M. I. Mangione, D. A. Heredia, E. N. Durantini, L. Otero and M. Gervaldo, *Sustainable Energy Fuels*, 2020, **4**, 6125–6140.

23 N. U. Day, C. C. Wamser and M. G. Walter, *Polym. Int.*, 2015, **64**, 833–857.

24 J. Durantini, G. M. Morales, M. Santo, M. Funes, E. N. Durantini, F. Fungo, T. Dittrich, L. Otero and M. Gervaldo, *Org. Electron.*, 2012, **13**, 604–614.

25 M. G. Walter and C. C. Wamser, *J. Phys. Chem. C*, 2010, **114**, 7563–7574.

26 H. Chen, J. Wang, W. Zhang, Y. Guo, Q. Ding and L. Zhang, *ACS Appl. Mater. Interfaces*, 2023, **15**, 12453–12461.

27 S. Cogal, M. Kiristi, K. Ocakoglu, L. Oksuz and A. U. Oksuz, *Mater. Sci. Semicond. Process.*, 2015, **31**, 551–560.

28 F. Zaar, S. Olsson, R. Emanuelsson, M. Strømme and M. Sjödin, *Electrochim. Acta*, 2022, **424**, 1406616.

29 E. Bermúdez Prieto, E. J. González López, C. A. Solis, J. C. Leon Jaramillo, L. P. Macor, R. E. Domínguez, Y. B. Palacios, S. Bongiovanni Abel, E. N. Durantini, L. A. Otero, M. A. Gervaldo and D. A. Heredia, *RSC Adv.*, 2024, **14**, 15929–15941.

30 B. Ballarin, R. Seeber, L. Tassi and D. Tonelli, *Synth. Met.*, 2000, **114**, 279–285.

31 J. E. Durantini, R. Rubio, C. Solis, L. Macor, G. M. Morales, M. I. Mangione, D. A. Heredia, E. N. Durantini, L. Otero and M. Gervaldo, *Sustainable Energy Fuels*, 2020, **4**, 6125–6140.

32 P. A. Liddell, M. Gervaldo, J. W. Bridgewater, A. E. Keirstead, S. Lin, T. A. Moore, A. L. Moore and D. Gust, *Chem. Mater.*, 2008, **20**, 135–142.

33 C. Y. Lin, Y. C. Hung, C. M. Liu, C. F. Lo, Y. C. Lin and C. L. Lin, *Dalton Trans.*, 2005, 396–401.

34 N. U. Day, M. G. Walter and C. C. Wamser, *J. Phys. Chem. C*, 2015, **119**, 17378–17388.

35 M. J. Frisch, G. W. Trucks, H. B. Schlegel, G. E. Scuseria, M. A. Robb, J. R. Cheeseman and G. Scalmani, *et al.*, *Gaussian 16*, Gaussian, Inc., 2016.

36 A. D. Becke, *J. Chem. Phys.*, 1992, **96**, 2155–2160.

37 C. Lee, W. Yang and R. G. Parr, *Phys. Rev. B: Condens. Matter Mater. Phys.*, 1988, **37**, 785–789.

38 P. J. Hay and W. R. Wadt, *J. Chem. Phys.*, 1985, **82**, 270–283.

39 W. R. Wadt and P. J. Hay, *J. Chem. Phys.*, 1985, **82**, 284–298.

40 P. J. Hay and W. R. Wadt, *J. Chem. Phys.*, 1985, **82**, 299–310.

41 S. Grimme, J. Antony, S. Ehrlich and H. Krieg, *J. Chem. Phys.*, 2010, **132**, 154104.

42 K. Momma and F. Izumi, *J. Appl. Crystallogr.*, 2011, **44**, 1272–1276.

43 E. Poverenov, M. Li, A. Bitler and M. Bendikov, *Chem. Mater.*, 2010, **22**, 4019–4025.

44 N. U. Day, M. G. Walter and C. C. Wamser, *J. Phys. Chem. C*, 2015, **119**, 17378–17388.

45 T. Ye, Y. He and E. Borguet, *J. Phys. Chem. B*, 2006, **110**, 6141–6147.

46 T. F. Guarr and F. C. Anson, *J. Phys. Chem.*, 1987, **91**, 4037–4043.

47 A. Bettelheim, B. A. White, S. A. Raybuck and R. W. Murray, *Inorg. Chem.*, 1987, **26**, 1009–1017.

48 J. Durantini, L. Otero, M. Funes, E. N. Durantini, F. Fungo and M. Gervaldo, *Electrochim. Acta*, 2011, **56**, 4126–4134.

49 R. Yewale, P. Damlin, M. Salomäki and C. Kvarnström, *Mater. Today Commun.*, 2020, **25**, 101398.

50 P. K. Jha, S. Kochrekar, A. Jadhav, R. Lassfolk, M. Salomäki, E. Mäkilä and C. Kvarnström, *Energy Storage Mater.*, 2024, **72**, 103758.

This journal is © The Royal Society of Chemistry 2025

J. Mater. Chem. C, 2025, **13**, 23577–23588 | **23587**

51 E. Tavakol, A. Kakekhani, S. Kavani, P. Tan, M. M. Ghaleni, M. A. Zaeem, A. M. Rappe and S. Nejati, *J. Am. Chem. Soc.*, 2019, **141**, 19560–19564.

52 A. Popov, B. Brasiunas, L. Mikoliunaite, G. Bagdziunas, A. Ramanavicius and A. Ramanaviciene, *Polymer*, 2019, **172**, 133–141.

53 S. M. Kuzmin, S. A. Chulovskaya, O. A. Dmitrieva, N. Z. Mamardashvili, O. I. Koifman and V. I. Parfenyuk, *J. Electroanal. Chem.*, 2022, **918**, 116476.

54 S. Marciniak, X. Crispin, K. Uvdal, M. Trzcinski, J. Birgerson, L. Groenendaal, F. Louwet and W. R. Salaneck, *Synth. Met.*, 2004, **141**, 67–73.

55 S. Kochrekar, A. Kalekar, S. Mehta, P. Damlin, M. Salomäki, S. Granroth, N. Meltola, K. Joshi and C. Kvarnström, *RSC Adv.*, 2021, **11**, 19844–19855.

56 E. Mitraka, M. J. Jafari, M. Vagin, X. Liu, M. Fahlman, T. Ederth, M. Berggren, M. P. Jonsson and X. Crispin, *J. Mater. Chem. A*, 2017, **5**, 4404–4412.

57 M. Boudiaf, Y. Liang, R. Lamare, J. Weiss, H. Ibrahim, M. Goldmann, E. Bentouhami, V. Badets, S. Choua, N. Le Breton, A. Bonnefont and L. Ruhlmann, *Electrochim. Acta*, 2019, **309**, 432–449.

58 M. Goll, A. Ruff, E. Muks, F. Goerigk, B. Omiecienski, I. Ruff, R. C. González-Cano, J. T. Lopez Navarrete, M. Carmen Ruiz Delgado and S. Ludwigs, *Beilstein J. Org. Chem.*, 2015, **11**, 335–347.

59 C. L. Gaupp and J. R. Reynolds, *Macromolecules*, 2003, **36**, 6305–6315.

60 I. Zozoulenko, A. Singh, S. K. Singh, V. Gueskine, X. Crispin and M. Berggren, *ACS Appl. Polym. Mater.*, 2019, **1**, 83–94.

61 B. Craig, P. Townsend, C. P. de Leon, C. K. Skylaris and D. Kramer, *Polymers*, 2024, **16**, 1376–1398.

62 C. Kvarnström, H. Neugebauer, S. Blomquist, H. J. Ahonen, J. Kankare and A. Ivaska, *Electrochim. Acta*, 1999, **44**, 2739–2750.

63 T. A. Welsh and E. R. Draper, *RSC Adv.*, 2021, **11**, 5245–5264.

64 Y. Hu, Z. Wang, K. Lin, J. Xu, X. Duan, F. Zhao, J. Hou and F. Jiang, *J. Polym. Sci., Part A: Polym. Chem.*, 2016, **54**, 1583–1592.

65 M. Gervaldo, M. Funes, J. Durantini, L. Fernandez, F. Fungo and L. Otero, *Electrochim. Acta*, 2010, **55**, 1948–1957.

66 H. Fu, Y. Tang, F. Zhan, L. Zhang, W. Zhan, Y. Dong, W. Li and C. Zhang, *Chem. Eng. J.*, 2023, **461**, 141848.

67 D. Mo, T. Tong, K. Deng and Q. Feng, *Electrochim. Acta*, 2024, **475**, 143654.

23588 | *J. Mater. Chem. C*, 2025, **13**, 23577–23588

This journal is © The Royal Society of Chemistry 2025